



# Effects of spatial configuration on contrast detection

Yoram Bonneh, Dov Sagi \*

*Department of Neurobiology, Brain Research, The Weizmann Institute of Science, Rehovot 76100, Israel*

Received 4 April 1997; received in revised form 16 October 1997; accepted 31 December 1997

---

## Abstract

We studied spatial integration at low contrasts by testing the detection thresholds of multi-Gabor element displays, examining configuration parameters such as orientation uniformity, contour smoothness, continuity, spacing and relative phase. We find that detectability depends on stimulus geometry and is constrained by collinearity and proximity spatial relationships. For textures, thresholds decrease with local orientation uniformity. For a ‘coherent’ contour (e.g. smooth and continuous), thresholds decrease linearly with increased number of elements, on a log–log scale, with a slope of  $-1/4$  (sensitivity  $S \propto N^{1/4}$ ). However, for a ‘non-coherent’ contour (e.g. jagged or with spacing  $> 5\lambda$ ) thresholds are only slightly affected by the number of patches. Similar behavior is observed for supra-threshold stimuli embedded in band-pass noise. These results suggest that contrast integration is primarily based on local mechanisms and constrained by contour properties. These local mechanisms are possibly mediated by lateral interactions in the primary visual cortex. © 1998 Elsevier Science Ltd. All rights reserved.

*Keywords:* Spatial summation; Lateral interactions; Long range connections; Contrast threshold; Perceptual grouping

---

## 1. Introduction

Psychophysical and physiological evidence suggest that the visual input is first decomposed by local analyzers or channels tuned to specific properties such as orientation, spatial frequency and direction of motion [1,2]. However, much less is known about the integration of these analyzers into coherent percepts. Integration between analyzers was examined in psychophysical summation-at-threshold experiments, where the detectability of a compound stimulus is compared with the detectability of its components. Studies of contrast summation show a linear summation within a channel [3] and a probability summation or an equivalent non-linear spatial pooling of channels [4] across space [5–7], spatial frequency [8–10], orientation [11], and time [12]. The probability summation model commonly used to interpret these results [7,13,14] assumes independent channels with high threshold (high enough to make false detection negligible) integrated by a global ‘inclusive or’ mechanism. An alternative model [4] assumes deterministic channels with a power transducer function and a global linear integrator with variability assumed

at a later stage. Different models were applied, making different assumptions on the role of noise (low versus high threshold) in pooling across channels, leading to different predictions, though not necessarily distinguishable by current data [15,16]. Regardless of the model assumed, independent detection within spatial channels predicts contrast summation between channels to be independent of spatial configuration.

Although current models assume channel independence, this assumption holds only to a first approximation (at least for supra-threshold stimuli) and interactions between channels have been described. Inhibitory and facilitatory interactions were found between neighboring channels on the spatial [17–19] and spatial frequency [20] dimensions. Attempts to isolate these effects [21] suggest iso-orientation short-range surround inhibition, possibly involved in orientation pop-out, and long-range collinear excitation possibly involved in contour integration. Parallel physiological and anatomical studies of striate cortex in cat and monkey revealed similar lateral interactions mediated by short- and long-range horizontal connections [22,23] showing iso-orientation surround inhibition [22,24,25] and collinear facilitation [26,27].

Other related psychophysical studies used high contrast band-pass stimuli to investigate spatial integration

---

\* Corresponding author. Tel.: +972 8 9343747; fax: +972 8 9344131; e-mail: dubi@nisan.weizmann.ac.il.

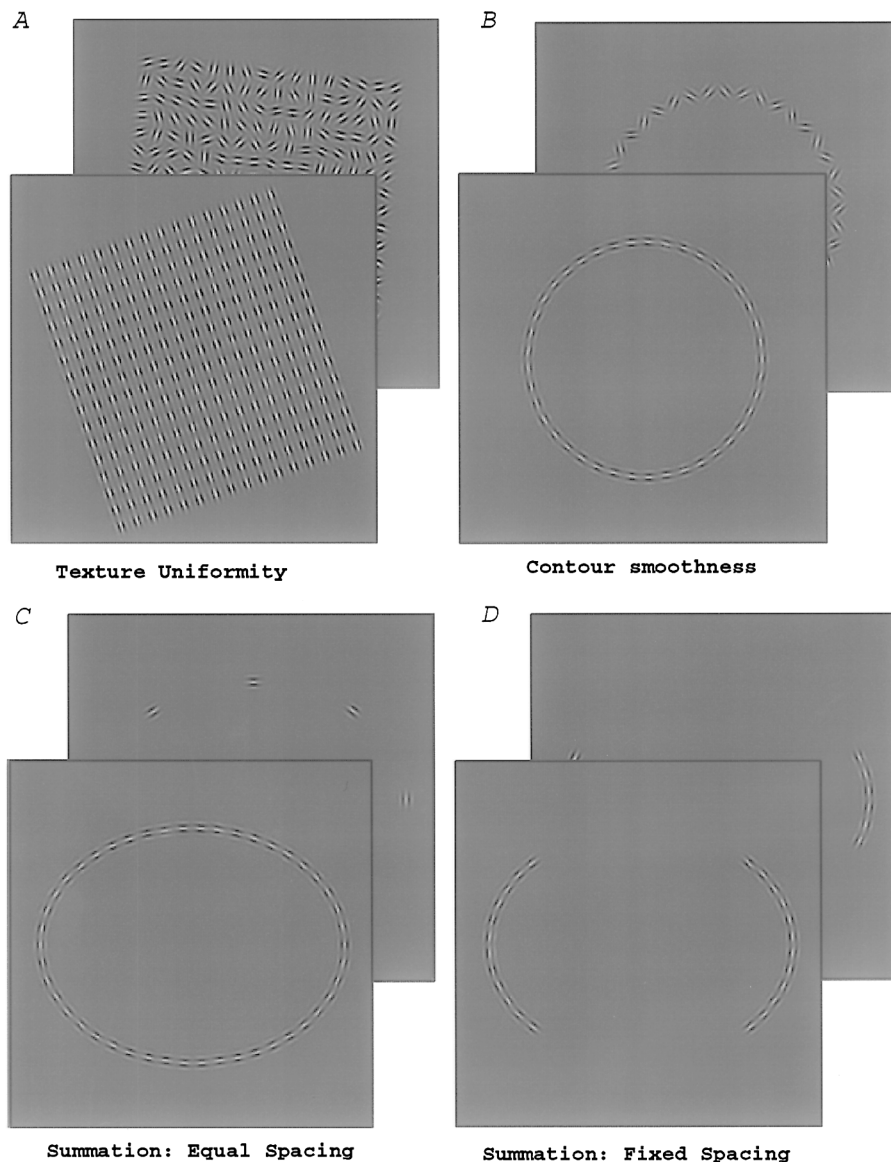


Fig. 1. Examples of stimuli used. Each pair of displays stands for a different experiment, with results showing lower thresholds for the foreground display. From left to right, top to bottom—texture orientation uniformity (A), contour orientation smoothness (B), distance effect in equal spacing (C) and distance effect in fixed spacing (D). Number of patches has been reduced, and their size relative to frame increased for clarity (60%).

according to Gestalt laws [28]. Field et al. [29] showed that the detectability of a contour made of high contrast band-pass elements (Gabor patches) aligned along a jagged path and embedded in the texture of randomly oriented elements, is affected by element alignment, path smoothness and inter-element spacing. They explained their results by assuming ‘local association fields’ between orientation tuned filters, possibly mediated by long-range connections in the primary visual cortex. Evidence for more global effects was also found in experiments involving detection of closed contours, with a closed path resulting in better detection rates than an opened one [30]. Furthermore, contrast sensitivity was found to be enhanced in the center of circular

closed contours and near the foci of elliptic contours [31]. These results can be accounted for by mutual interactions between local, orientation tuned, spatial filters providing the necessary medium for activity propagation within closed contours, though the use of high contrast stimuli may allow for other processes, involving higher level features, to take place.

In this paper we investigate the effect of spatial configuration on contrast detection thresholds and contrast summation. We use configurations of Gabor patches, both 2D textures and 1D contours (Fig. 1) to study the effect of orientation uniformity, contour smoothness, spacing and relative phase. Theories assuming independent local processing, predict sensitivity

to be independent of configuration. According to these theories, spatial integration, if it exists, is due to statistical (probability) summation and thus independent of spatial relations. We find that detectability depends on stimulus geometry and is constrained by collinearity and proximity spatial relationships, so that a ‘coherent’ configuration (e.g. smooth contour) is more easily detected than a ‘non-coherent’ one (e.g. spaced or jagged contour).

We complete the study by showing that the proximity and contour smoothness constraints for summation hold for supra-threshold stimuli embedded in band-pass noise.

## 2. Methods

### 2.1. Apparatus

Stimuli were displayed as gray-level modulation on Mitsubishi HL-7965 KW and Sony GDM 2000 TC color monitors, using a Silicon Graphics Reality Engine system. The video format was 60 Hz non-interlaced with  $1280 \times 1024$  pixels occupying a  $13 \times 10.4^\circ$  area. An 8-bit RGB mode was used and Gamma correction applied to produce a linear behavior of the displayed luminance. Note that thresholds for small Gabor signals, as used here, are high enough (5–40%) to be effectively measured with 8-bits gray-level resolution. The mean display luminance was  $40 \text{ cd/m}^2$  in an otherwise dark environment. Stimulus generation and display was controlled by THE SGI Crimson/Reality Engine workstation.

### 2.2. Stimuli

Stimuli consisted of multi-element Gabor displays of different configurations and sizes. The luminance profile of one vertical Gabor patch is given by the product of a sinusoidal carrier of wavelength  $\lambda$  and a Gaussian envelope of S.D.  $\sigma$  in the  $(x, y)$  space of the image

$$G(x, y) = \cos\left(\frac{2\pi}{\lambda}x + \phi\right) \exp\left(-\frac{x^2 + y^2}{\sigma^2}\right)$$

In all sub-threshold experiments we used the same Gabor parameters  $\lambda = \sigma = 0.08^\circ$  of visual angle, equivalent to a spatial frequency of 12.5 cycles/ $^\circ$  with an envelope width of 1.39 cycles at half height. The phase  $\phi$  was 0 except for the alternating phase condition (phase of neighboring patches is alternated between 0 and  $180^\circ$ ). For the single experiment with supra-threshold stimuli we used  $\lambda = \sigma = 0.12^\circ$  equivalent to a 8.33 cycles/ $^\circ$  frequency. Other stimulus parameters are specific for each experiment and described in Section 3.

### 2.3. Experimental procedures

A two-alternative-forced choice paradigm was used in all experiments. Each trial consisted of two stimuli presented sequentially, only one of which had a target. Before each trial, a small fixation circle was presented at the center of the screen. When ready, the observer pressed a key activating the trial sequence: a no-stimulus interval (0.3 s), a first stimulus presentation, a no-stimulus interval with fixation (1.1 s total, 0.5 s with fixation), and a second stimulus presentation. In all experiments, the duration of stimulus presentation was 117 ms. The observer was asked to perform a detection task, i.e. to determine which of the stimuli contained the target.

Each block consisted of 50 trials on average, across which the Gabor signal configuration was kept constant. Screen luminance was kept constant during the trials. The stimuli were viewed binocularly from a distance of 150 cm in a dark environment. Auditory feedback, by means of a keyboard bell, was given immediately after an erroneous response.

Target threshold contrast (which ranged from 5 to 40%) was determined by a staircase method, which was shown to converge to 79% correct [32]. In this method, the target contrast is increased by 0.1 log units ( $\approx 26\%$ ) after an erroneous response and decreased by the same amount after three consecutive correct responses. The number of contrast reversals (change from increase to decrease or vice versa) within each block was counted, and the block was terminated after eight such reversals. Threshold contrast of a block was the geometric average of the last six reversals (the first two were ignored). Threshold results of four to nine blocks were averaged to compute a mean threshold and the standard error of the mean (S.E.) plotted in the figures.

A variation of the above procedure was used to measure contrast threshold for a single Gabor patch in different positions simultaneously. This was done with a ‘mixed staircase’ procedure, where trials from different positions were randomly mixed keeping a separate staircase for each position. In this way, the observer is uncertain about the target position and cannot use eye movements to improve performance. In all other respects, the procedure is identical to a sequential set of blocks.

In all experiments, observers were instructed to keep fixation at the center without moving their eyes.

### 2.4. Data analysis

To compute power-law fits to the summation data while taking into account the local sensitivity measures, we used a weighted power-law according to the following formula:

$$S = \left( \sum_i S_i^q \right)^{1/q}$$

where  $S_i = 1/C_{t_i}$  is the sensitivity at position  $i$ ,  $C_{t_i}$  the contrast threshold,  $q$  is the exponent constant and  $S$  is the global sensitivity. The value of the exponent constant  $q$  was selected by least-squares error (difference between predicted and measured thresholds) minimization. The sensitivity at each position and orientation was computed from the sampled (three orientations in eight positions) sensitivity measures by interpolation. This formulation of the power-law fit is identical to the vector summation [4] and the high-threshold probability summation [7] formulations, although it is used here as an empirical fit, rather than a theoretical prediction.

### 2.5. Observers

Four observers (GH, RP, OY, AL) and one of the authors (YB) participated in the experiments. The observers, high school and undergraduate students (between the ages of 16 and 25), except for YB, were naive as to the purpose of the experiments, and were paid in return. All observers had normal or corrected-to-normal vision.

## 3. Results

### 3.1. Orientation uniformity effect on texture threshold

The effect of orientation uniformity on contrast detection thresholds of Gabor textures was measured by varying the local orientation randomization level, with randomized global orientation. Assuming independent processing of local elements at contrast threshold level, results are not expected to be affected by orientation uniformity.

#### 3.1.1. Stimuli

Gabor texture configuration,  $24 \times 24$  elements ( $6^\circ \times 6^\circ$ ) in size,  $3\lambda$  inter-element spacing. Local Gabor orientation randomization range was varied between blocks from 0 (all orientations equal to global orientation) to  $+90^\circ$  (random orientation). Global orientation of the whole configuration was randomized between trials. See example in Fig. 1A. A high contrast temporal cue (circle,  $5^\circ$  in radius), was displayed with each stimulus presentation. Block order was randomized between sessions.

#### 3.1.2. Results

Results are presented in Fig. 2 for observers GH, RP and YB. Normalized contrast threshold (log units) is plotted as a function of orientation randomization range (0 for iso-orientation, 180 for full  $\pm 90^\circ$  randomization). Values are normalized by the detection

threshold of a single randomly oriented foveal patch. Results show that the uniform configuration is more easily detected, as thresholds increase by 0.2 log units with increasing randomization. Note that the threshold for about 600 randomly oriented patches is only 15–30% lower than the threshold for a single central patch, while that of the uniform texture is about half of it.

The results are unlikely to be due to threshold differences between orientations and positions, since local orientation is always randomized (in the uniform case it is done indirectly by global randomization between trials). Uncertainty as for the configuration (uniform or random) does not affect the results. Results from mixed blocks (trials from different configurations selected at random with separated staircases) show the same effect.

### 3.2. Contour smoothness effects on contrast threshold

The effect of contour smoothness on detection threshold was measured by varying the local Gabor orientation in a circular arrangement of patches. Here, the important factor is the local patch orientation relative to the circle tangent line at its position (see Fig. 1B).

#### 3.2.1. Stimuli

A circle of Gabor patches, centered at fixation,  $30\lambda$  in radius,  $3\lambda$  inter-element spacing, ( $\lambda = \sigma = 0.08^\circ$ ), occupying total of  $5^\circ$  of visual field. In one set of experiments, full circles were used and local patch orientations, relative to contour tangent, were varied between blocks from  $0^\circ$  ('smooth') to  $45^\circ/135^\circ$  ('star-

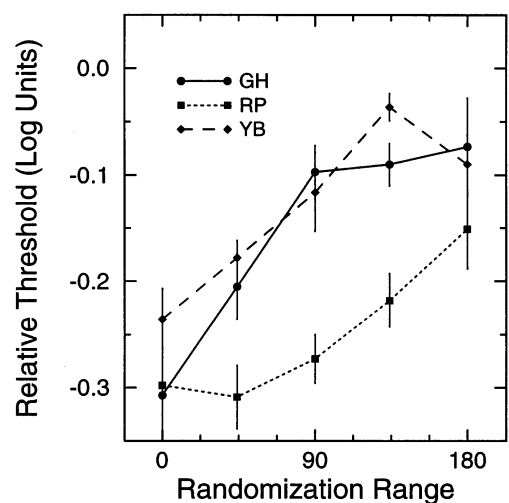


Fig. 2. Orientation uniformity effect on texture detection threshold. Normalized contrast thresholds are plotted as a function of orientation randomization range (0 for iso-orientation,  $\pm 90^\circ$  for full randomization) for observers GH, RP and YB. Values are normalized by the detection threshold of a single randomly oriented central patch. Each datum point is based on six to eight measurements. Error bars indicate 1 S.E. For all observers, threshold increases with increased randomization.

shaped') and 90° tangential (termed 'sun-shaped' circle, though it may look more like a set of parallel patches arranged on a circle). An example for the 'smooth' and the 'star-shaped' circles appear in Fig. 1B. Note that the term 'smooth' is used specifically to denote co-circular elements and thus the 90° tangential condition ('sun-shaped') is not considered smooth. The effect of phase was tested by repeating the experiments with alternating phase of neighboring patches (0 and 180°).

In another set of experiments, we tested arcs of circles with different number of patches and two orientation conditions: smooth (co-circular) and random local orientation. The patches were positioned as two arcs of the circle on the left and right side. The number of patches and their orientations were fixed within block and varied between blocks (orientations were re-randomized between blocks in the random orientation condition). An example for stimuli similar to those used in the 'smooth' condition appears in Fig. 1D (the stimuli were circular rather than elliptic as in the figure). On each session we measured the detection threshold of two vertical patches, 30λ in periphery along the horizontal meridian, for normalization. Block order was randomized between sessions.

### 3.2.2. Results

Effects due to local contour orientation continuity are shown in Fig. 3. Normalized contrast thresholds are plotted as a function of deviations from the tangential angle (0 for collinear, 45 for star-shaped, 90 for sun-shaped). Separate plots are shown for uniform phase and alternate phase conditions (for observers GH and AL) and for all observers and phases averaged ( $N = 4 \times 2$ ). Threshold values are normalized by the threshold for detecting two vertical peripheral patches. Lowest thresholds are obtained with smooth circles (0), highest for star-shaped circles (45), with sun-shaped circles producing intermediate thresholds. The magnitude of the effect, i.e. the difference between smooth and star-shaped conditions is 0.15–0.2 log units, for both uniform and alternating phase conditions.

Orientation effects on summation along fragments of a circle are depicted in Fig. 4. Contrast threshold is plotted as a function of the number of patches on a log–log scale relative to the threshold of two patches (from two sides of the horizontal axis) for three observers (GH, YB and RP) and two configurations: smooth (co-circular) and random local orientation. Results show a significant difference between 'smooth' and 'random' configurations for all observers. Spatial contrast summation for the smooth configuration appears linear on a log–log scale with a magnitude of 0.3 log units between two patches and 62 patches (summation slope of  $-1/5$ ). Spatial summation for the random configuration is smaller for GH and almost absent for YB and RP.

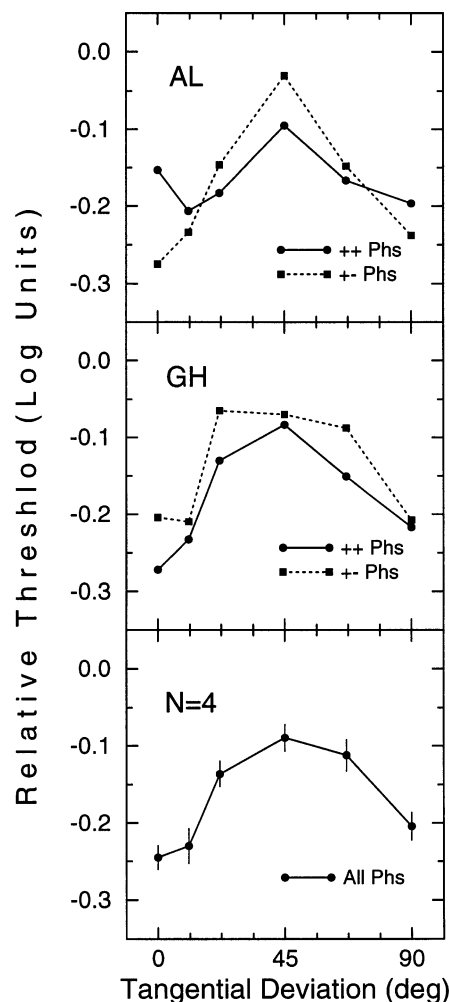


Fig. 3. Local orientation effects on circular contour thresholds. Normalized contrast threshold is plotted as a function of orientation deviation from the contour tangent (0 for collinear, 45 for star-shaped, 90 for sun-shaped, see examples). Separate plots are shown for uniform (+ +) and alternate (+ -) phase conditions (for observers GH and AL) and for all four observers averaged. Each datum point is based on four to six measurements for individual observers and 20–30 measurements for the four observer average. Error bars indicate 1 SE. Values are normalized by the threshold of detecting two vertical peripheral patches.

In order to verify that the effect is not due to a non-uniform sensitivity, we measured thresholds in eight different positions and three orientations along the circular contour using a mixed-staircase procedure (see Section 2). The results show no significant difference between orientations but a clear difference between positions. Points of same eccentricity along the horizontal meridian were more sensitive than points along the vertical meridian (with difference as much as 0.25 log units). We used these sensitivity measures to compute a weighted power-law fit to the data (see Section 2). These fits appear as a solid line in each graph (Fig. 4) and correspond to sensitivities along the smooth configuration (sensitivities along the random

configuration are very similar and produce a similar curve, not shown). The estimated exponent constants are  $q = 3.7$  for observer GH,  $q = 4.1$  for YB and  $q = 4.2$  for RP. The fits are slightly curved due to the unequal sensitivity (patches were added from left/right towards top/bottom) and match the experimental data for the smooth configurations, while deviating dramatically from the random configuration curves. More details about the sensitivity mapping and summation fits can be found in [33].

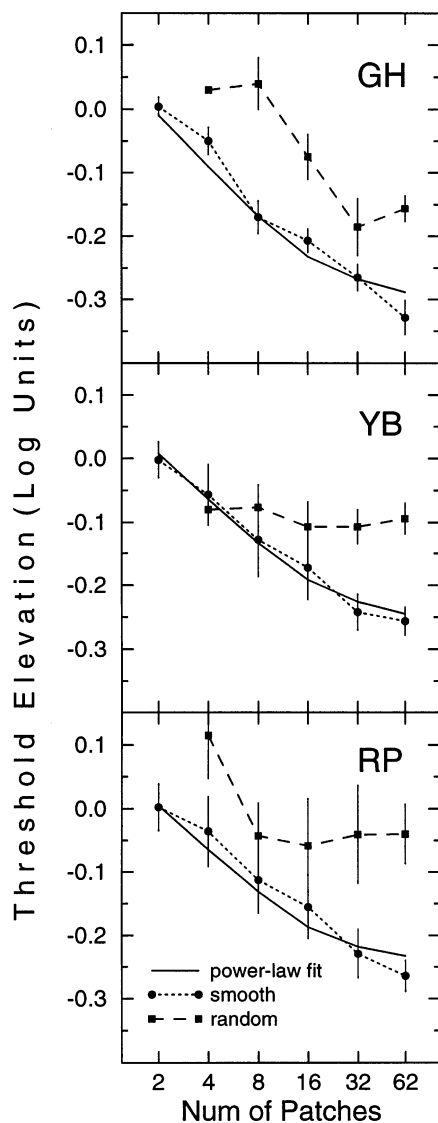


Fig. 4. Contour summation for smooth and random circular configurations. Detection thresholds are plotted as a function of number of patches on a log–log scale, relative to the threshold for two patches (observers GH, YB and RP). Solid lines show weighted power-law fits (exponent constant  $q = 3.7$  for GH,  $q = 4.1$  for YB and  $q = 4.2$  for RP) for the smooth circle. Each datum point is based on four to nine measurements, except from the two extreme points (two and 62 patches) which are based on 10–15 measurements. Error bars indicate 1 SE.

### 3.3. Inter-element distance effects on contrast threshold

The effect of inter-element distance was measured using two methods: (i) equal distance along an elliptic contour with varied number of patches and (ii) fixed inter-element distance for some discrete distance values. The aspect ratio of the ellipses was chosen so that the contrast sensitivity of isolated Gabor signals was approximately constant along its contour.

#### 3.3.1. Stimuli

Elliptic arrangement of Gabor patches making a smooth contour around fixation (ellipse axis =  $4.8^\circ \times 6.24^\circ$ ) with varied number of patches and inter-element distance. In the ‘equal spacing’ condition, the patches were equally spaced along the contour and varied in number between blocks (see example in Fig. 1C). In the ‘fixed spacing’ condition, fixed distances were used ( $3\lambda$ ,  $5\lambda$ ,  $8\lambda$ ) with the varied number of patches occupying two lateral (left and right) fragments of the ellipse (see example in Fig. 1D).

#### 3.3.2. Results

Results are shown in Fig. 5. Contrast thresholds (relative to the threshold of two patches) are plotted as a function of the number of patches on a log–log scale, for the two spacing conditions (equal and fixed) and for two observers (GH and YB). Results for the two extreme points (two and 73 patches) for the two spacing conditions were pooled together since they correspond to identical stimuli and did not vary significantly.

Results for the fixed-spacing condition (left) show an approximately linear behavior on a log–log scale for  $3\lambda$  spacing, with a slope of around  $-1/4$ , which could be described as ‘fourth-root summation’ (sensitivity  $S \propto N^{1/4}$ ). However, thresholds are consistently higher with less summation for the  $5\lambda$  and  $8\lambda$  spacings (with effects magnitude of 0.1–0.15 at  $5\lambda$  and 0.2 log units at  $8\lambda$ ). Results for the equally spaced configurations (right) indicate little summation (0.1 log units) up to 32 patches ( $6.8\lambda$  spacing) but improve rapidly, by 0.2 log units, between  $5\lambda$  (45 patches) and  $3\lambda$  (full ellipse) spacing. Finally, the two spacing conditions produced comparable thresholds at the two extreme points as expected (being identical stimuli), but while the  $3\lambda$  spacing summation is compatible with a fourth-root summation rule, the equal spacing curves show much less summation at long distances, reflecting the role of proximity in contrast summation.

We fit the data with a weighted power-law based on local sensitivity measures along the elliptic contour as done for the circles in the previous experiment (solid lines in Fig. 5). The computed least-squares exponent constants for the  $3\lambda$  fixed-spacing condition are  $q = 4.0$  for GH and  $q = 4.7$  for YB. These exponents are used to compute the estimated summation curves for both

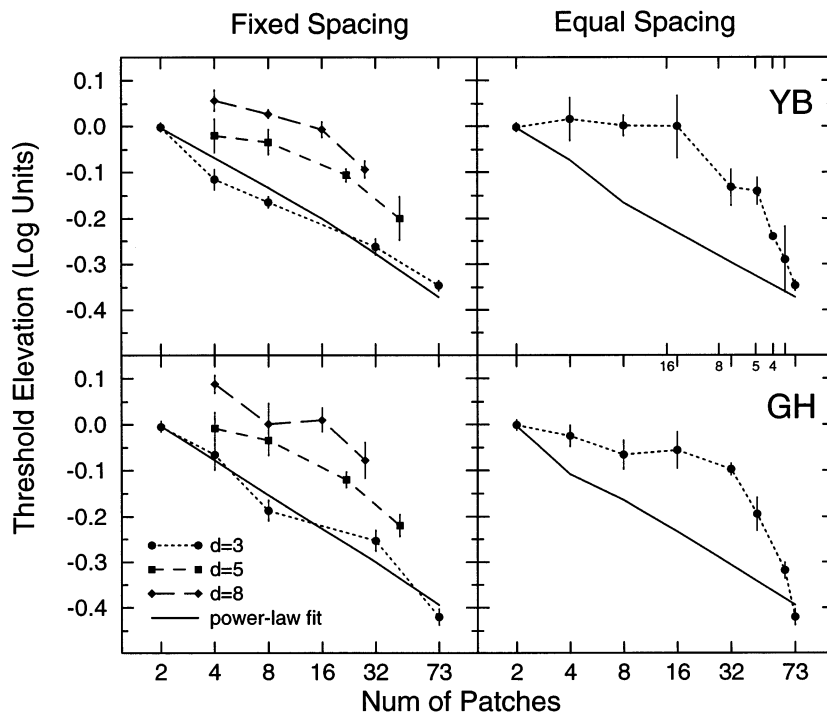


Fig. 5. The effect of inter-element distance on contrast detection threshold. Detection threshold (relative to the threshold of two patches) is plotted as a function of the number of patches on a log–log scale. Right—equal spacing between patches along the elliptic configuration. Left—fixed spacing (3, 5,  $8\lambda$ ) along left and right side fragments of the ellipse. Solid lines denote weighted power-law fits (exponent constant  $q = 4.0$  for GH and  $q = 4.7$  for YB) computed for the  $3\lambda$  fixed-spacing configuration from contrast thresholds of single patches at different positions. The small numbers in the middle axis of the right graph denote inter-element spacing in  $\lambda$  units. Each datum point is based on three to seven measurements, except from the value for two patches (used for normalization) which is based on 30–50 measurements. Error bars indicate 1 SE. Observers are GH (bottom) and YB (top).

the fixed and equal-spacing conditions, each based on its corresponding sensitivities. Since the elliptic contour is almost iso-sensitive, these fits are almost linear on the log–log scale (slope  $\approx -1/4$ ) regardless of configuration. They show a good fit to the fixed  $3\lambda$  spacing curve, while strongly deviating from the equal-spacing data.

The effect of proximity is better demonstrated in Fig. 6, where summation exponent constants ( $q$  values corresponding to a  $-1/q$  slope on a log–log scale) estimated from the equal-spacing data are plotted as a function of inter-element spacing, assuming uniform sensitivity. Note that  $q$  increases rapidly with inter-element distance and reaches  $q = 6$  for distances of  $5\lambda$  and above. Interestingly, thresholds obtained for equally spaced ‘star-shaped’ configurations (not plotted) are similar to those of the ‘smooth’ configuration when considering large distances, but are 0.15–0.2 log units higher for short distances (below  $4\lambda$ ). Thus, contour smoothness seems to affect summation only when short inter-element distances are considered.

The effect of the spatial configuration on the psychometric function was tested by measuring psychometric functions for smooth and star-shaped  $3\lambda$  spaced ellipses and for two peripheral patches. Results show that the log–log slope of the psychometric function does not

depend on the configuration nor on the number of patches, but is strongly influenced by the experimental paradigm (e.g. mixing trials of different contrasts within a block). Thus, no relation between the psycho-

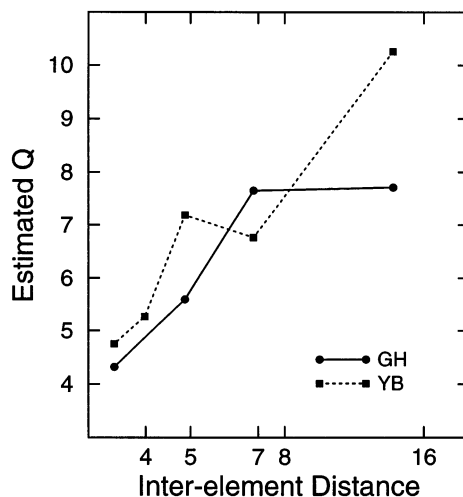


Fig. 6. The summation exponent constant  $q$  of the power-law fit (denoting slope of  $-1/q$  on a log–log scale) as a function of inter-element distance ( $\lambda$  units) as computed from equal spacing thresholds for the elliptic configuration. Homogeneous sensitivity is assumed. Observers are GH and YB. Note that  $q$  grows rapidly and reaches  $q = 6$  for  $5\lambda$  distance.

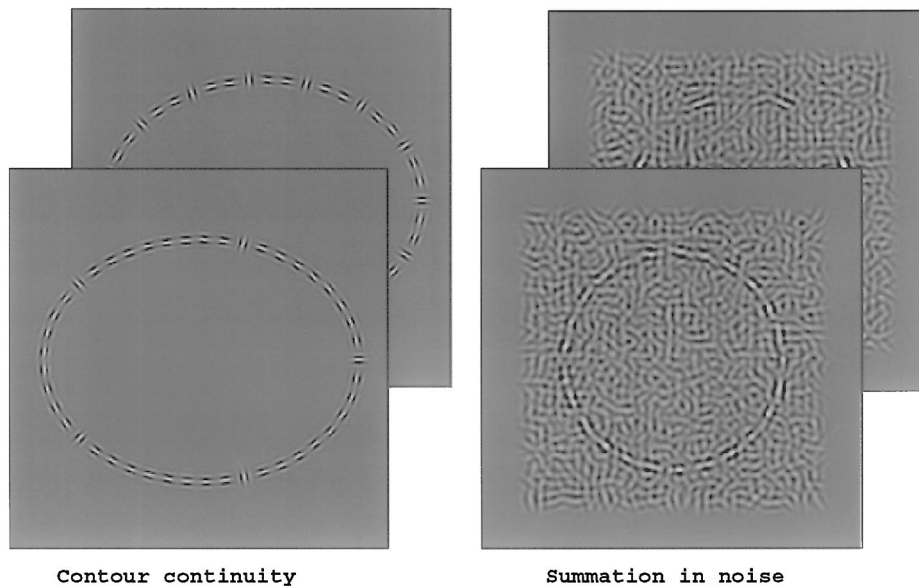


Fig. 7. Examples of stimuli used to test continuity (left) and summation in the presence of noise (right). Continuity is tested by setting delimiters (orthogonal patches) that break the contour into clusters. Stimuli with clusters of ten patches (foreground, easy) and three patches (background, more difficult) are demonstrated. Summation in the presence of noise is demonstrated with a full circle (foreground, easy) and an equally spaced eight patch circle (background, more difficult). The number of patches for the continuity stimuli has been reduced, and their size relative to frame increased for clarity (60%).

metric function slope and the summation exponent was found, which is inconsistent with theories that assume such a relation [4,7]. More details on the measured psychometric functions can be found in [33].

### 3.4. Breaking a continuous contour

The results of the previous experiments suggest that local proximity and contour smoothness constrain contrast summation. It is possible that integration is carried out globally (e.g. via probability summation) once some local conditions are met (e.g. via size-limited linear integration mechanism), or alternatively, that local spatial relations modulate activity propagation along the contour so that breaking it into subparts could degrade summation. We test the importance of contour continuity by adding orthogonal patches as delimiters into a smooth elliptic contour.

#### 3.4.1. Stimuli

Smooth elliptic arrangement of Gabor patches around fixation ( $\lambda = \sigma = 0.08^\circ$ , ellipse axis =  $4.8^\circ \times 6.24^\circ$ ) with a fixed number of 70 patches equally spaced (inter-element distance is  $3.13\lambda$ ). A number of delimiters (orthogonal patches) were inserted in place of contour patches with equal contrast and spacing along the contour. The number of delimiters was varied between blocks so that each block tested a different inter-delimiter spacing or cluster size (see example in Fig. 7 left).

#### 3.4.2. Results

Results are presented in Fig. 8. Threshold elevation, relative to the contrast threshold of a smooth contour, is plotted as a function of cluster size (including one delimiter), where cluster size of 70 stands for a smooth

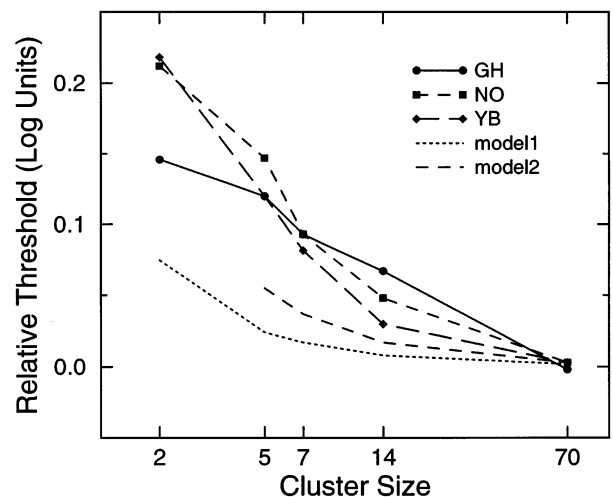


Fig. 8. Effects of breaking a smooth contour. Threshold elevation is plotted as a function of cluster size (including one delimiter) on a log–log scale for observers GH, NO and YB. For all three observers, threshold increases with decreased cluster size. For comparison, fourth-root summation (exponent of  $-1/4$ ) when delimiters are excluded (model 1) and twice the number of delimiters excluded (model 2) are depicted. Each datum point is based on four to six measurements for observers NO and YB and over 20 measurements for observer GH.

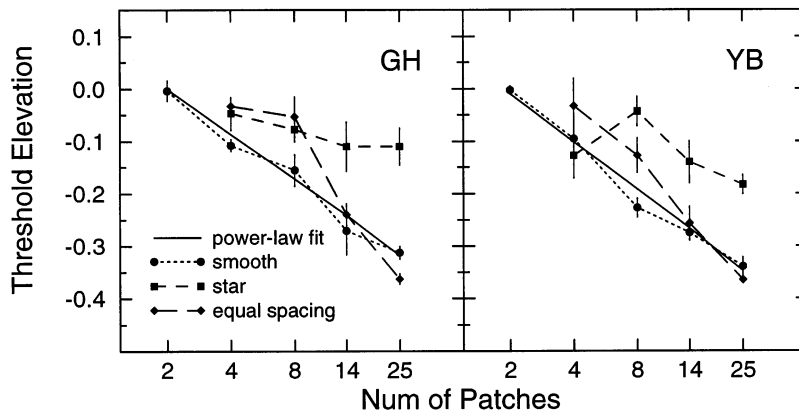


Fig. 9. The effect of spacing and local orientation on summation in noise. Detection threshold is plotted as a function of the number of patches on a log–log scale relative to the threshold of two patches, for two observers and for three conditions: smooth and star-shaped fixed spacing ( $3\lambda$ ) and equal spacing configurations. Computed least-squares power-law fits (exponents  $-1/3.5$  for GH and  $-1/3.3$  for YB) are plotted as solid lines. Each datum point is based on three to four measurements. Error bars indicate 1 SE.

contour (no delimiters) and cluster size of two for an alternating arrangement (same number of delimiters and contour patches). For all three observers, threshold was found to increase with increasing delimiter number (i.e. decreasing cluster size). The difference between the two extreme cases is about 0.2 log units being equivalent to the effect of the star-shaped contour (see Fig. 3), reflecting the local smoothness constraint described in the previous experiments. However, here threshold elevation is obtained for larger clusters as well, e.g. a 0.1–0.15 log units effect for five-patch clusters, pointing to some global shape effects.

In order to check whether the effect can be explained by removal of some local contributions to summation, we examine two simple models. The first (model 1) assumes that fourth-root summation with equal sensitivity taking place without counting the delimiters. It is clear that this model cannot account for the data (Fig. 8), as discounting the delimiters yields very little threshold elevation (0.024 for the 14 delimiters/five-patch cluster). The second model (model 2) assumes that each delimiter affects two locations, so that twice the number of delimiters are discounted. This yields a larger effect (0.05 log units for the five-patch cluster) but not large enough to match the experimental results (0.12–0.15 log units). Thus, the delimiters seem to degrade summation by more than expected from the removal of their contributions to any local mechanism and this indicates a summation mechanism based on activity propagation.

### 3.5. Contrast summation in the presence of noise

Previous studies of supra-threshold detection found no contrast summation beyond one cycle for a foveal grating buried in a white noise mask [34], no area summation for a peripheral ( $10^\circ$ ) Gabor patch displayed on a sustained grating pedestal of the same

frequency [35] and no length summation for a Gaussian bar displayed on a long sustained Gaussian bar pedestal [36]. These studies suggest that supra-threshold and sub-threshold summation behave differently. Here we test whether the configuration dependent summation found in the present experiments apply to supra-threshold stimuli as well.

#### 3.5.1. Stimuli

Circular arrangements of Gabor patches around fixation,  $12\lambda$  in radius ( $\lambda = \sigma = 0.12^\circ$ ), occupying total of  $3^\circ$  of visual field, embedded in band-pass noise mask. The noise mask consisted of 1225 same but randomly oriented 16% contrast Gabor patches, with spacing of  $1\lambda \pm 0.2\lambda$  (uniform jitter) and was added to the circular configuration target (thus, the mask was transiently presented with the target). Five masks were prepared in advance for each block and selected at random except that the two masks in a single 2AFC trial were never the same. Local orientation, inter-element distance and element number were manipulated as in the sub-threshold experiments for three summation conditions: Summation along fixed ( $3\lambda$ ) inter-element distance smooth circle (as demonstrated in Fig. 1D for similar sub-threshold stimuli), Summation along a similar star-shaped circle ( $45^\circ/135^\circ$  tangential) and Summation for equally spaced elements along a smooth circle (see example in Fig. 7 right).

#### 3.5.2. Results

Results are presented in Fig. 9. Contrast threshold is plotted as a function of the number of patches on a log–log scale relative to the threshold of two patches for the three summation conditions and for two observers (GH and YB). The results are similar to those obtained for the sub-threshold summation. Summation in the fixed spacing smooth condition follows log–log

linear dependency, roughly consistent with the fourth-root summation rule. The computed least-squares power-law fits appear as solid lines, and were computed assuming equal sensitivity (actual sensitivity was not measured). The computed exponent constants are  $q = 3.5$  for GH and  $q = 3.3$  for YB. In comparison, the equal spacing plot clearly deviates from the power-law fit (0.1 log units effect) for spacing larger than  $5.3\lambda$  (the spacing for the 14 patch configuration) and so does the summation for the star-shaped condition which shows 0.2 log units less summation for a full circle.

These results demonstrate that contrast summation operates for supra-threshold stimuli in a similar way as for low contrast stimuli and perhaps even more effectively ( $q = 3.5$ , though eccentricity and spatial frequency are different).

#### 4. Discussion

In this study we investigated the effect of spatial configuration on contrast detection thresholds and on contrast summation of multi-band-pass stimuli (Gabor signals). We find that texture thresholds decrease with local orientation uniformity (Fig. 2) and circular contour thresholds decrease with contour ‘smoothness’ regardless of phase differences (Fig. 3).

Contrast summation was measured for different contours and compared with the measured local sensitivity (single patch) along each contour. We find that for increasing number of patches, thresholds decrease linearly on a log–log scale with a slope of  $-1/4$  (sensitivity  $S \propto N^{1/4}$ ) provided that proximity, smoothness and continuity constraints are met. When these constraints are violated, as in the case of widely spaced ( $> 4\lambda$ ), or with non-smooth (e.g. random orientation) configurations, thresholds are much less affected by patch number ( $q > 8$ ). Similar behavior is observed for supra-threshold stimuli embedded in band-pass noise.

##### 4.1. Limiting conditions for spatial summation

Our results suggest that spatial relations such as proximity, smoothness and continuity put constraints on spatial summation. We consider the unconstrained summation and the different factors that put constraints on it in turn.

##### 4.2. The fourth-root summation rule

The maximal summation we observed (both sub- and supra-threshold) is consistent with a fourth-root summation rule. Summation exponent of around  $1/4$  fits the sub-threshold data with some differences across observers while the exponent for supra-threshold summation is slightly higher ( $1/3.5$ ). These results are similar to

those obtained previously with a grating strip and accounted for by probability summation [7]. Interestingly, a similar fourth-root summation was observed for the detection of speed differences [37] and in our preliminary study of summation effects in contrast discrimination (see below). Thus, the fourth-root summation appears to be a general rule and poses a challenge for a unified explanation.

##### 4.2.1. Proximity

Summation drops rapidly with decreasing proximity between  $3\lambda$  and  $8\lambda$  (0.15 log units effect relative to a  $q = 4$  power-law, Fig. 5) and corresponding summation exponent constants increase from  $q = 4$  to  $q = 6$  (Fig. 6). Proximity is expressed in wavelength units, though we have only tested 12 cycle/° stimuli (except from supra-threshold stimuli with 9 cycle/°). The dependence of spatial interaction range on the wave length was previously demonstrated [18].

##### 4.2.2. Smoothness

Contour smoothness was tested as deviation from co-circularity along a fixed radius circle. Decreasing smoothness provides a relatively gradual decrease in summation, as compared with the fast degrading effect of proximity (Fig. 3).

##### 4.2.3. Continuity

Continuity was tested by breaking a smooth contour with a number of orthogonal delimiters. The result is a threshold elevation that increases with the number of delimiters, indicating activity propagation along the contour. The system appears not to be able to integrate over disconnected clusters even when each cluster is a ‘good’ configuration, i.e. summation is possible within clusters (or objects) but is limited between them. It is possible, however, that probability summation between larger clusters could take place.

##### 4.2.4. Eccentricity

For the sub-threshold experiments, we used peripheral stimuli  $2.5$ – $3^\circ$  in eccentricity. Preliminary experiments with  $1^\circ$  eccentricity did not yield similar effects of reduced summation, perhaps because of the fewer number of elements. However, an eccentricity of  $1.5^\circ$  is sufficient to get a clear effect with supra-threshold stimuli embedded in band-pass noise (Fig. 9). Preliminary results with more peripheral stimuli,  $7^\circ$  in eccentricity, show a similar (0.2 log units) difference between smooth and star-shaped elliptic configurations, which indicates that similar mechanisms for contour integration at threshold are operative in the periphery (but see [38]).

#### 4.2.5. Phase

The contour smoothness effect we have measured is insensitive to phase polarity (0 or 180), as alternating the phase of neighboring patches yields roughly the same thresholds (Fig. 3). This result is consistent with previous lateral masking studies using line stimuli [39,40] or Gabor signals [21,41] which show contrast polarity invariant facilitation with high-contrast masks at large separations ( $> 3\lambda$ ).

#### 4.3. Supra-threshold contrast summation

Previous studies of supra-threshold detection found very limited summation for foveal grating embedded in noise [34] and for a peripheral Gabor patch on top of a grating pedestal [35]. Our results show the same fourth-root summation behavior and the same configuration effects for supra-threshold stimuli embedded in band-pass noise. To account for the seemingly contradicting results, note that the previous studies used 2D grating patterns, while we use 1D contours of Gabor patches. It is possible that iso-orientation surround inhibition found both physiologically [22,24] and psychophysically [42,43], with increasing strength at high contrasts [25,43,44] suppresses filter activity and reduces summation. This explanation is consistent with a recent finding of configuration effects in short duration binocular rivalry [43] which shows a clear difference between regions and borders with high contrast uniform regions found to be suppressed while smooth contours to be enhanced. Other factors that may affect the different results are retinal inhomogeneity [34] and the use of sustained pedestal [35].

While our results imply contrast summation within objects, as indicated by the smoothness constraints, and not between objects, recent studies involving motion discrimination indicate the opposite. Verghese and Stone [37,45,46]; see also [47] found increasing motion discrimination sensitivity with increasing number of Gabor signals ( $q = 3.5$ ) but not with increasing signal size. Our preliminary study [48] of size-dependent contrast discrimination, using high contrast Gabor signals, supports size-independent contrast discrimination thresholds, however, only when both target and pedestal sizes are increased—increasing target size while keeping a constant large pedestal produces contrast summation ( $q = 3.5$ ). Thus, it seems that increasing pedestal size permits lateral inhibitory interactions [17,49,50] to reduce discrimination thresholds in a way that produces an approximated size-independent discrimination threshold.

#### 4.4. Underlying mechanisms

Current models used to account for summation-at-threshold results are the probability summation

[7,13,14], the vector summation [4] and the signal detection theory-based models [15,16]. All models assume global integration of either statistically independent or deterministic channels, ignoring local spatial relations. Thus, the current data presents a paradox to these models; if each detector contributes to the decision independently, the pattern of summation could not depend on the spatial relationship between local elements. In explaining the data, we can rule out the involvement of non-optimal detectors (e.g. of lower frequency) since contrast is just below threshold for the optimal detectors and the inter-element distance is always large enough ( $> 3\lambda$ ) to minimize integration within a receptive field of a standard detector [21]. As our results show spatial summation independent of phase relationships, the effect can not be attributed to integration within first-stage linear filters.

A possible alternative is to explain the critical proximity range and collinearity constraints using second-stage filters that integrate multiple elements within their receptive fields. Accordingly, the little summation observed beyond the critical range is explained by probability summation, e.g. with very high uncertainty [15,16]. However, this scheme cannot account for the fourth-root summation observed for proximal and collinear elements, because whatever local mechanism is used, the long-range integration beyond the size of the largest mechanism is based on repeated instances of this mechanism combined with the limited probability summation. In order to explain the long-range integration that spans a substantial part of a curved contour (ellipse in our experiments) with feed forward mechanisms, one would require to assume a hierarchical scheme. Such a scheme has been recently proposed to explain the linear summation observed for orientation information in concentric, random-dot Glass patterns [51].

A more feasible model to consider is channel interaction as the summation mechanism. This idea is based on accumulating physiological and psychophysical evidence for lateral interactions in V1 [22,23,25] and more specifically, local collinear enhancement [26,27,52]. These findings are consistent with the current effects of proximity, smoothness and continuity. On this account, the summation we observed reflects integration of a weighting function corresponding to the strength of lateral interaction. Assuming a reasonable weighting function (exponential, Gaussian), we have recently found that a simple network with local lateral excitatory connections can account for the observed fourth-root summation as well as for the proximity and collinearity constraints [53].

An important implication of the channel interaction explanation is that channels are not independent at threshold, suggesting that the detectability of different patches should be correlated. Correlated detection is

supported by observers reports that at contrast threshold, large parts of a ‘good’ configuration are observed and only few patches from a ‘bad’ one. Correlated detectability, if indeed exists, may reflect homogeneous activity rates and/or temporal correlation. In both cases, a network of lateral connections mediating contour integration is assumed as suggested by Gilbert [22], where excitatory connections may enhance firing rates and generate correlated activity. Activity correlation is consistent with the temporal correlation hypothesis for visual feature integration [54] and may explain the increased summation, as synchronization is known to improve neural integration [55]. Alternatively, the network may produce enhanced homogeneous activities corresponding to regional summation, with detectability determined by any individual detector (further integration is not useful since detectors response is correlated).

### Acknowledgements

We thank Marius Usher, Christopher Tyler, Yael Adini, Yasuto Tanaka, Uri Polat and Alexander Cooperman for helpful discussions. This work was supported by the Basic Research Foundation administered by the Israel Academy of Sciences and Humanities.

### References

- [1] DeValois RL, DeValois KK. Spatial Vision. Oxford: Oxford University Press, 1990.
- [2] Graham N. Visual Pattern Analyzers. Oxford: Oxford University Press, 1989.
- [3] Kulikowski J, Abadi R, King-Smith P. Orientation selectivity of grating and line detectors in human vision. *Vis Res* 1973;13:1479–86.
- [4] Quick RF. A vector-magnitude model of contrast detection. *Kybernetik* 1974;16:65–7.
- [5] Legge GE. Space domain properties of a spatial frequency channel in human vision. *Vis Res* 1978;18:959–69.
- [6] Howell ER, Hess RF. The functional area for summation to threshold for sinusoidal gratings. *Vis Res* 1978;18:369–74.
- [7] Robson JG, Graham N. Probability summation and regional variation in contrast sensitivity across the visual field. *Vis Res* 1981;21:409–18.
- [8] Graham N, Robson JG, Nachmias J. Grating summation in fovea and periphery. *Vis Res* 1978;18:815–26.
- [9] Quick RF, Mullins WW, Riechert TA. Spatial summation effect on two-component grating thresholds. *J Opt Soc Am* 1978;68:116–21.
- [10] Graham N, Robson JG. Summation of very close spatial frequencies: The importance of spatial probability summation. *Vis Res* 1987;27:1997–2007.
- [11] Phillips GC, Wilson HR. Orientation bandwidths of spatial mechanisms measured by masking. *J Opt Soc Am A* 1984;1:226–32.
- [12] Watson AB. Probability summation over time. *Vis Res* 1979;19:515–22.
- [13] Sachs MB, Nachmias J, Robson JG. Spatial frequency channels in human vision. *J Opt Soc Am* 1971;61:1176–86.
- [14] Wilson HR, Bergen JR. A four mechanism model for threshold spatial vision. *Vis Res* 1979;19:19–32.
- [15] Pelli DG. Uncertainty explains many aspects of visual contrast detection and discrimination. *J Opt Soc Am A* 1985;2:1508–32.
- [16] Tyler CW. Threshold psychophysics, probability summation and the analysis of spatial summation behavior. Prepublished web paper ([www.ski.org/CWTyler\\_lab/CWTyler/PrePublications/ProbSumm/ProbSumm.html](http://www.ski.org/CWTyler_lab/CWTyler/PrePublications/ProbSumm/ProbSumm.html)), 1997.
- [17] Sagi D, Hochstein S. Lateral inhibition between spatially adjacent spatial frequency channels? *Percept Psychophys* 1985;37:315–22.
- [18] Polat U, Sagi D. Lateral interaction between spatial channels: suppression and facilitation revealed by lateral masking experiments. *Vis Res* 1993;33:993–9.
- [19] Adini Y, Sagi D, Tsodyks M. Excitatory-inhibitory networks in the visual cortex, psychophysical evidence. *Proc Natl Acad Sci USA* 1997;94:10426–31.
- [20] Tolhurst D, Barfield L. Interaction between spatial frequency channels. *Vis Res* 1978;18:951–8.
- [21] Zenger B, Sagi D. Isolating excitatory and inhibitory non-linear spatial interactions in contrast detection. *Vis Res* 1996;36:2497–513.
- [22] Gilbert CD. Horizontal integration and cortical dynamics. *Neuron* 1992;9(1):1–13.
- [23] Malach R, Amir Y, Bartfeld E, Grinvald A. Relationship between intrinsic connections and functional architecture revealed by optical imaging and in vivo targeted biocytin injections in primate visual cortex. *Proc Natl Acad Sci USA* 1993;90:10469–73.
- [24] Blakemore C, Tobin EA. Lateral inhibition between orientation detectors in the cat’s visual cortex. *Exp Brain Res* 1972;15:439–40.
- [25] Grinvald A, Lieke EE, Frostig RD, Hildesheim R. Cortical point-spread function and long range interactions revealed by real-time optical imaging of macaque monkey primary visual cortex. *J Neurosci* 1994;14:2545–68.
- [26] Kapadia MK, Ito M, Gilbert CD, Westheimer G. Improvement of visual sensitivity by changes in local context: parallel studies in human observers and in vl of alert monkeys. *Neuron* 1995;15:843–56.
- [27] Polat U, Norcia AM. Neurophysiological evidence for contrast dependent long range facilitation and suppression in the human visual cortex. *Vis Res* 1996;36:2099–109.
- [28] Koffka K. Principles of Gestalt Psychology. New York: Harcourt Brace World, 1935.
- [29] Field DJ, Hayes A, Hess RF. Contour integration by the human visual system: Evidence for a local association field. *Vis Res* 1993;33:173–93.
- [30] Kovács I, Julesz B. A closed curve is much more than an incomplete one: Effect of closure in figure-ground segmentation. *Proc Natl Acad Sci USA* 1993;90:7495–7.
- [31] Kovács I, Julesz B. Perceptual sensitivity maps within globally defined visual shapes. *Nature Lond* 1994;370:644–6.
- [32] Levitt H. Transformed up-down methods in psychoacoustics. *J Acoust Soc Am* 1971;49:467–77.
- [33] Bonneh Y, Sagi D. Effects of spatial configuration on contrast detection. Tech Rep GC-DS/97-1, The Weizmann Institute of Science, 1997.
- [34] Kersten D. Spatial summation in visual noise. *Vis Res* 1984;24:1977–90.
- [35] Tyler CW. Does visual probability summation exist? *Invest Ophthalmol Vis Sci* 1995;36 Suppl. 5905.
- [36] Tyler CW. Is supra-threshold visual processing purely punctate? *Invest Ophthalmol Vis Sci* 1996;37 Suppl. 5912.

- [37] Verghese P, Stone LS. Combining speed information across space. *Vis Res* 1995;35(20):2811–23.
- [38] Hess RF, Dakin SC. Absence of contour linking in peripheral vision. *Nature* 1997;390:602.
- [39] Yu C, Levi DM. Spatial facilitation predicted with end-stopping spatial filters. *Vis Res* 1997;37(22):3117–27.
- [40] Wehrhahn C, Dresf B. Detection facilitation by collinear stimuli in humans: Dependence on strength and sign of contrast. *Vis Res* 1998;38(3):423–8.
- [41] Ishai A, Sagi D. Visual imagery facilitates visual perception: psychophysical evidence. *J Cogn Neurosci* 1997;9:476–89.
- [42] Andriessen JJ, Bouma H. Eccentric vision: adverse interactions between line segments. *Vis Res* 1976;16:71–8.
- [43] Bonnef Y, Sagi D. Configuration saliency revealed in short duration binocular rivalry. *Vis Res* (in press).
- [44] Stemmler M, Usher M, Niebur E. Lateral interactions in primary visual cortex: A model bridging physiology and psychophysics. *Science* 1995;269:1877–80.
- [45] Verghese P, Stone LS. Perceived visual speed constrained by image segmentation. *Nature* 1996;381:161–3.
- [46] Verghese P, Stone LS. Spatial layout affects speed discrimination. *Vis Res* 1997;37(4):397–406.
- [47] Braddick O. Only one speed per object. *Nature* 1996;381:117–8.
- [48] Bonnef Y, Sagi D. Contrast integration across space. *Invest Ophthalmol Vis Sci* 1998 Suppl. 5859.
- [49] Allman J, Miezin F, McGuinness E. Stimulus specific responses from beyond the classical receptive field. *Annu Rev Neurosci* 1985;8:407430.
- [50] Chubb C, Sperling G, Solomon J. Texture interactions determine apparent lightness. *Proc Natl Acad Science USA* 1989;86:9631–5.
- [51] Wilson HR, Wilkinson F, Asaad W. Concentric orientation summation in human form vision. *Vis Res* 1997;37:2325–30.
- [52] Polat U, Sagi D. The architecture of perceptual spatial interactions. *Vis Res* 1994;34:73–8.
- [53] Bonnef Y, Usher M, Sagi D, Hermann M. Mechanisms for spatial integration in visual detection: a model based on lateral interactions. Tech Rep GC-DS/97–6, The Weizmann Institute of Science, 1997.
- [54] Singer W, Gray CM. Visual feature integration and the temporal correlation hypothesis. *Annu Rev Neurosci* 1995;18:555–86.
- [55] Abeles M. *Corticonics*. Cambridge, UK: Cambridge University Press, 1991.